International Journal of Clean Coal and Energy, 2015, 4, 1-10
Published Online February 2015 in SciRes. http://www.scirp.org/journal/ijcce
http://dx.doi.org/10.4236/ijcce.2015.41001

Microstructural Degradation of Thermal Barrier Coatings on an Integrated Gasification Combined Cycle (IGCC) Simulated Film-Cooled Turbine Vane Pressure Surface Due to Particulate Fly Ash Deposition

Kevin Luo[1], Andrew C. Nix[1], Edward M. Sabolsky[2]

[1]Department of Mechanical and Aerospace Engineering, Center for Alternative Fuels, Engines and Emissions, Morgantown, USA
[2]Department of Mechanical and Aerospace Engineering, Morgantown, USA
Email: kluo1@mix.wvu.edu, andrew.nix@mix.wvu.edu

Received 18 October 2014; revised 17 November 2014; accepted 10 December 2014

Abstract

Research is being conducted to study the degradation of thermal barrier coatings (TBC) employed on IGCC turbine hot section airfoils due to particulate deposition from contaminants in coal synthesis gas (syngas). West Virginia University (WVU) had been working with US Department of Energy, National Energy Technology Laboratory (NETL) to simulate deposition on the pressure side of an IGCC turbine first stage vane. To simulate the contaminant deposition, several TBC coated, angled film-cooled test articles were subjected to accelerated coal fly ash, which was injected into the flow of a combustor facility with a high pressure (approximately 4 atm) and a high temperature (1560 K) environment. To investigate the degradation of the TBCs due to particulate deposition, non-destructive tests were performed using scanning electron microscopy (SEM) evaluation and energy dispersive X-ray spectroscopy (EDS) examinations. The SEM evaluation was used to display the microstructure change within the layers of the TBC system directly related to the fly ash deposition. The SEM micrographs showed that deposition-TBC interaction made the YSZ coating more susceptible to delamination and promoted a dissolution-reprecipitation mechanism that changed the YSZ morphology and composition. The EDS examination provided elemental maps of the shallow infiltration depth of the fly ash and chemical composition spectrum results which showed yttria migration from the YSZ into the deposition.

How to cite this paper: Luo, K., Nix, A.C. and Sabolsky, E.M. (2015) Microstructural Degradation of Thermal Barrier Coatings on an Integrated Gasification Combined Cycle (IGCC) Simulated Film-Cooled Turbine Vane Pressure Surface Due to Particulate Fly Ash Deposition. *International Journal of Clean Coal and Energy*, **4**, 1-10. http://dx.doi.org/10.4236/ijcce.2015.41001

Keywords

Thermal Barrier Coatings, Coal Syngas, IGCC Gas Turbine, Fly Ash Deposition, Microstructure

1. Introduction

In an effort to improve the efficiency and durability of gas turbines, research and development of TBC coating systems are being conducted worldwide. Thermal barrier coatings (TBCs) are applied onto gas turbine components and are designed to withstand high operating temperatures. The main function of the TBC is to extend the life of the gas turbine components while allowing for higher operating temperatures. The top layer of a TBC system typically contains the ceramic top coat comprised of partially stabilized zirconia, ZrO_2, with yttria (7 - 8 wt% Y_2O_3). The composition is typically termed as YSZ [1]. The two typical TBC application methods are air plasma sprayed (APS) and electron-beam physical-vapor deposition (EB-PVD). Although an APS coating has a lower thermal conductivity (*k*) value, an EB-PVD coating is typically preferred for its strain tolerance [2]. The 7YSZ phase constitution is the non-transformable, metastable tetragonal (t') phase, which provides stability at the high operating temperatures. For the as-deposited TBC coatings, a metallic bond coat (BC) is applied to the super alloy substrate prior to the application of the ceramic top coat. This BC coat is responsible for the adhesion between the top coat and the substrate and for providing an aluminum reservoir for the formation of alumina, α-Al_2O_3, in the thermally grown oxide (TGO). TGO grows between the bond coat and the ceramic top coat during thermal operation. Due to the TBC's low thermal *k* relative the substrate, it provides thermal insulation for the gas turbine components, allowing the turbine to operate at much higher gas temperatures than the melting point of the substrate material. This consequentially increases the gas turbine efficiency.

The increase in the turbine operating temperatures has resulted in several issues for the TBC. One issue is the degradation of TBCs from contaminants that become molten. The molten deposits can degrade the components in the turbines or inhibit external cooling designs. The deposits in the gas turbines are due to impurities that enter through the inlet air or the upstream combustion of particulate laden alternative duels such as coal-derived synthesis gas (syngas).

One common form of molten deposit that can degrade TBC systems is known as calcium-magnesium-alumino-silicate (CMAS). The deposits from CMAS are from siliceous debris (sand) that enter through the air intake. Once the temperatures exceed 1150˚C, the ingested particles and debris melt and adhere onto the surface of the ceramic top coat. Levi, Hutchinson, Vidal-Sétif, and Johnson [3] found that CMAS deposits de-stabilized the non-transformable, metastable tetragonal t'-YSZ top coat of an electron beam-physical vapor deposition (EB-PVD) TBC and infiltrated the intercolumnar gaps of the top coat towards the TGO. As the CMAS infiltrates and cools, the stress mismatch between the glassy deposits and the YSZ can lead to spallation of the TBC. In a separate CMAS study, Wellman and Nicholls [4] found that CMAS can cause severe damage to the EB-PVD YSZ column morphology from dissolution, change the YSZ crystal structure from tetragonal to monoclinic from depletion in yttria, and erode the TBC system. The morphology change can cause a reduction in the insulating properties and strain tolerance of the TBC.

Another form of deposit which can degrade TBCs is derived from the intake of volcanic ash. Drexler *et al.* [5] found that volcanic ash ingested by jet engines was found to damage conventional APS YSZ thermal barrier coatings. The eruption of Eyjafjallajökull volcano in Iceland in 2010 created volcanic ash clouds in which a jet aircraft inadvertently can fly through. The ash from Eyjafjallajökull was found to form a glass at roughly 1160˚C. The nature of the damage was similar to degradation caused by molten CMAS, where the molten ash was able to infiltrate the pores and cracks of the top coat causing enhanced microstructural change and final spallation.

The purpose of the current study is to understand the effects of particulate deposition due to coal syngas combustion in a high-pressure, high-temperature environment on the microstructure of thermal barrier coatings on film-cooled gas turbine components. To model the fly ash particulate, deposition experiments were conducted in the National Energy Technology Laboratory (NETL) Aerothermal Test Facility to simulate 10,000 operating hours of syngas contaminant intake on first stage vane components. This was performed using a 6-hour test on angled test articles [6]. The accelerated deposition process takes place at a pressure of approximately 4 atm and

a gas temperature of 1560 K. Processed fly ash was injected into the test section using a high pressure particulate seeding system in which the Stokes number and particulate loading is matched between the laboratory and engine conditions.

Improving the gas turbine durability and efficiency requires an understanding of the effects of particulate deposition on the thermal barrier coatings. The current study examines the influence of the fly ash deposition on the microstructure of the TBC layers using scanning electron microscopy (SEM) and energy dispersive X-ray spectroscopy (EDS).

2. Test Articles and Experimental Methods

In the current study, the test articles were designed to simulate the pressure side of a first stage turbine vane at incline angles of 10˚ and 20˚. The design of the test articles are described in the work by Murphy, Nix, Lawson, Straub, and Beer [6]. Each test article is fabricated out of HAYNES 230 (HA230) alloy and has four 3.9 mm diameter cooling holes placed on the face at a 30˚ to the surface. The cooling holes are scaled to 8× the size of an actual turbine vane cooling hole using Reynolds similarity. The cooling holes are connected to a high pressure air system which delivers cold air to the face of the test articles.

Each test article has a TBC applied using a directed vapor deposition (DVD) process [7]. A 7% Yttrium Stabilized Zirconia (7YSZ) coating with an approximate thickness of 400 µm is applied as the ceramic top coat of the TBC. The bond coat of the TBC system was ϒ-ϒ’ platinum aluminide (PtAl) with an approximate thickness of 15 - 20 µm. The ϒ-ϒ’ PtAl bond coat closely matches the phase properties of the nickel-based superalloy and was developed by Brian Gleeson at the University of Pittsburgh [8]. A shallow trench, a configuration commonly used in modern gas turbine components, is created by masking the cooling holes during the coating process [9]. **Figure 1** displays the two angled test articles after the TBC was applied [6].

The fly ash processing is described in a study by Murphy, Nix, Lawson, Straub, and Beer [6]. The processed fly ash has a mean particle size of 13 µm and the composition of the bituminous fly ash is given in **Table 1** [6] Unlike previous molten deposit and TBC studies where the molten deposit was formed by applying a paste onto the TBC and heat treated, the ash particulate was injected into a high pressure and high temperature facility and impacted onto the TBC coated test articles. Bons, Ameri, and Fletcher found that bituminous fly ash that is injected in a similar fashion experiences a volumetric decrease when it becomes molten and from sintering [10]. Lawson and Thole [11] used a Stokes number analysis between the laboratory and engine conditions given by Dennis, Shelton, and Le [12] to scale the particle inertial characteristics and set the desired mean particle di-

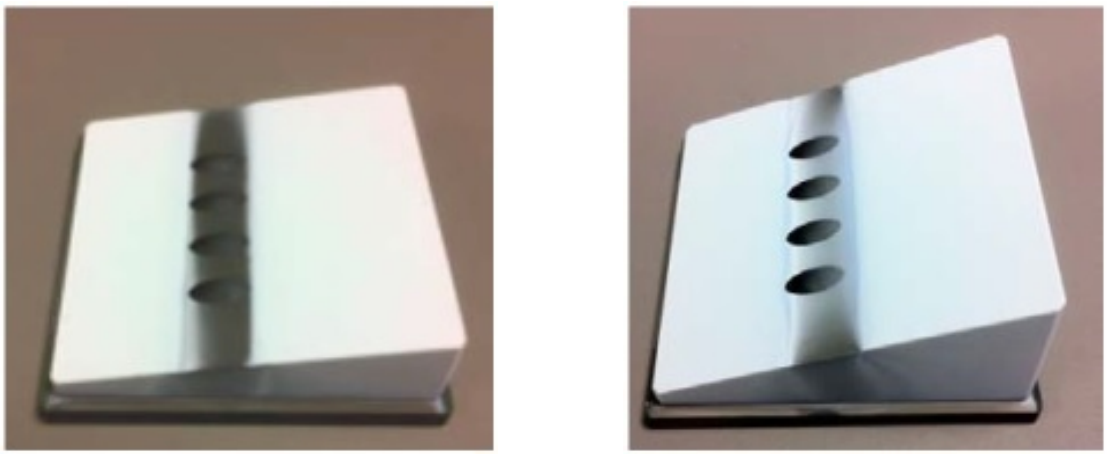

(a) (b)

Figure 1. Photographs of the (a) 10˚ and (b) 20˚ test articles with TBC before the deposition testing [7].

Table 1. Bituminous coal ash composition [7].

Oxides:	SiO_2	CaO	Fe_2O_3	Al_2O_3	SO_3	K_2O
wt.%	53.8	4.39	8.87	25.35	1.15	2.23

ameter. Lastly, the particulate loading is matched at 200 ppmw-hr to simulate 10,000 hours of particulate deposition into an engine in a 6-hour laboratory experiment [6].

The results from the study found that deposition formed on only one side of the test articles. Deposit formation on only one side of the test articles was due to a large deposit structure forming on the transition piece of the test section upstream of the test articles [13] [14]. The deposit structure on the test section transition piece created aswirl effect. This promoted an uneven distribution of fly ash into the test section and would be unrealistic in a first stage vane flow of an actual gas turbine.

The test articles used in this study are labeled and shown in **Figure 2** [15] The test article most heavily infiltrated was the 20-degree angled test article 1 (see **Figure 2(a)**). **Figure 2(b)** & **Figure 2(c)** contains images of the unexposed 20-degree angled test article 2 and the exposed 10-degree angled test article 3 respectively. To determine the effect of the fly ash deposition on the cross-sectional microstructure of the TBC, the test articles were sectioned into materials testing samples. The sectioning job produced flat test samples with an approximate thickness of 1/4 inches. **Figure 3** details the sample labels for each test article [15]. The heavy deposition on test article 1 is outlined in **Figure 3(a)**.

Prior to any SEM and EDS work, the samples undergo a micro-indentation procedure on the ceramic top coat to evaluate the effects on the mechanical properties from the fly ash deposition. The study found that the modulus of elasticity increases in areas where the molten deposition had cooled and adhered onto the top coating [15]. The increase in the surface stiffness can be directly related to the reduction in strain tolerance of the YSZ coating. Once micro-indentation was completed, SEM micrographs of the top view of the YSZ coatings (unexposed and deposition exposed) were taken, and then the samples were mounted, polished, and underwent microstructural analysis through scanning electron microscopy (SEM) examinations to provide high resolution images of the cross sections of the samples. Following SEM evaluation, energy dispersive X-ray spectroscopy (EDS) examinations of the ceramic top coat were conducted for determination of the elemental composition and mapping of the regions of interest (Hitachi S-4700).

3. Results and Discussion

SEM and EDS Results

Microstructural characterization examinations commenced after the micro-indentation work was completed. **Figure 4** contains images of unexposed test sample 2-3 and deposition exposed test sample 1-3 and their corresponding cross-sectional SEM micrograph of the TBC layers. The columnar structure of the DVD YSZ can be seen in both cross-sectional views of the samples. The DVD ceramic coating exhibited a higher density than the EB-PVD YSZ found in CMAS studies by Wellman and Nicholls [4] and Peng *et al.* [16] The only difference between the unexposed cross-sectional area in **Figure 4(a)** and the cross-section of the deposition exposed sample in **Figure 4(b)** at 250× magnification is the growth of TGO thickness (~5 μm) and intercolumnar and internal pores due to sintering. The lack of significant microstructural changes away from the top of the YSZ coating meant the deposition had a shallow infiltration depth.

SEM micrographs of the top view of unexposed and exposed YSZ coatings are shown in **Figure 5** [15]. **Figure 5(a)** shows the top view of an unexposed, as-deposited YSZ coating on test sample 2-1. The columnar structure produced by the DVD application process has inter-columnar gaps which improves the lateral strain

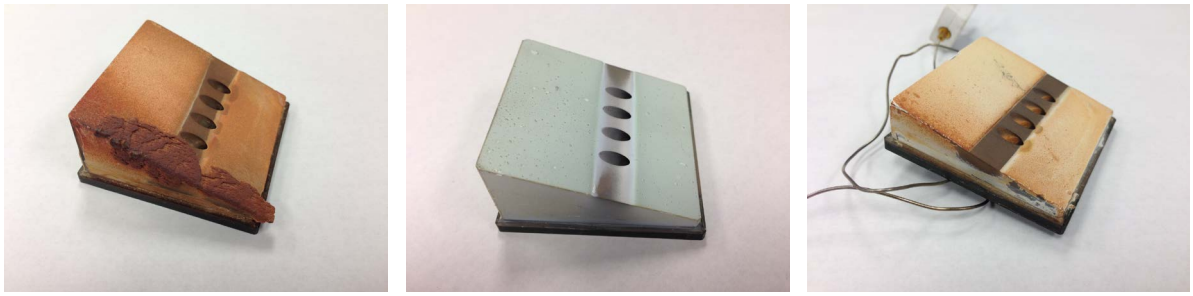

(a) (b) (c)

Figure 2. Labels of (a) Test Article 1—20˚ with deposition; (b) Unexposed Test Article 2—20˚; and (c) Test Article 3—10˚ with deposition [15].

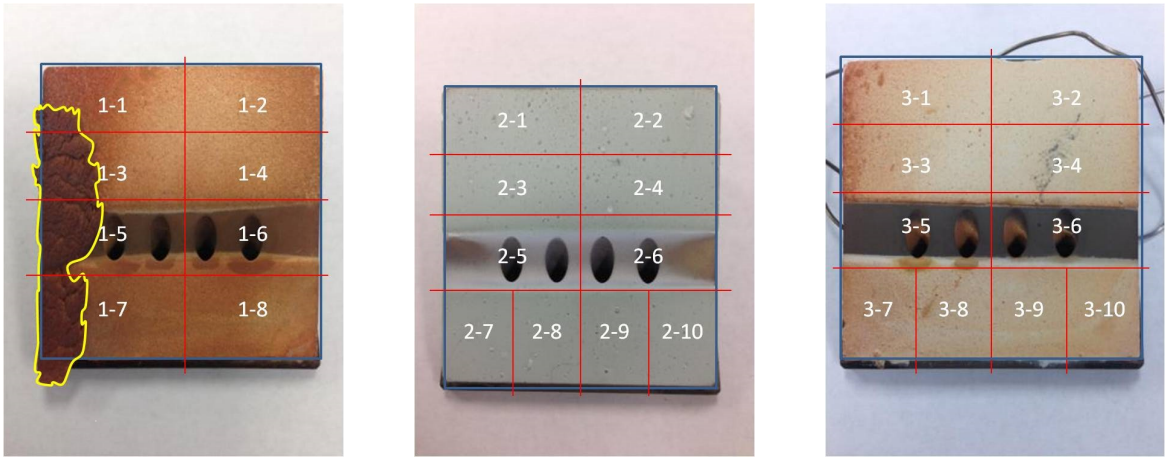

(a) (b) (c)

Figure 3. Sectioning diagrams and sample labels for (a) Test Article 1; (b) Test Article 2; and (c) Test Article 3 [15].

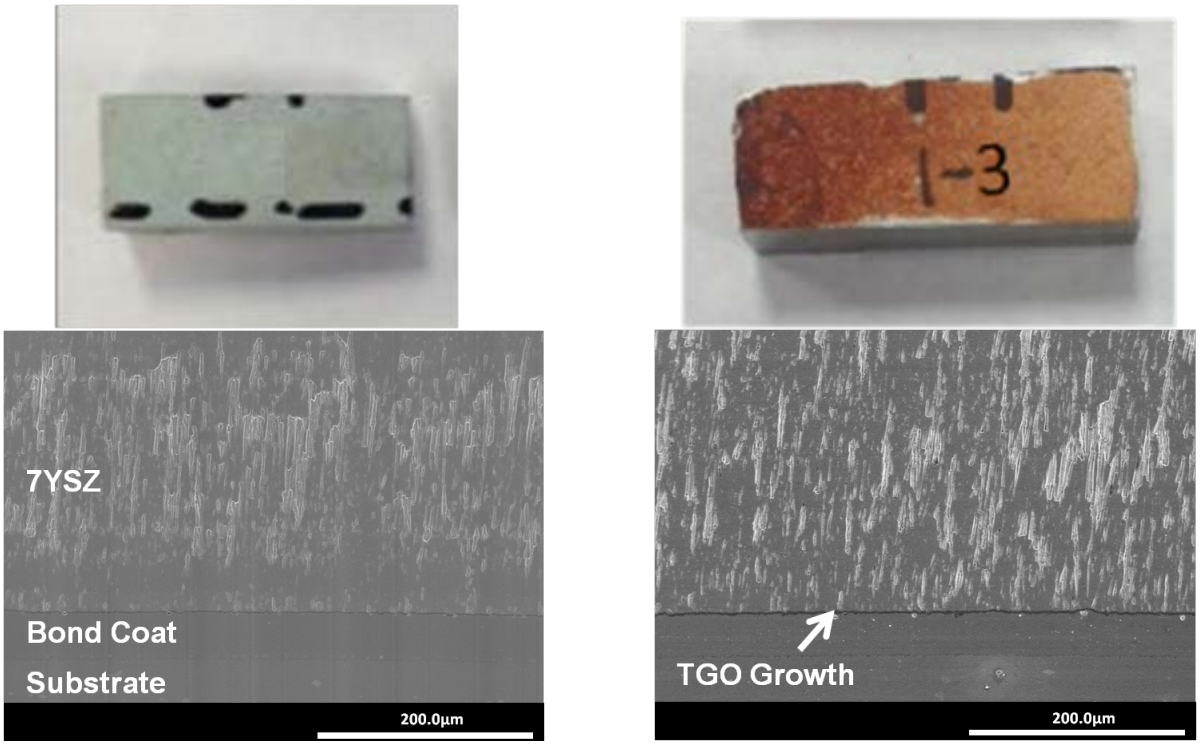

(a) (b)

Figure 4. Cross-section SEM micrograph of the (a) Unexposed sample 2-3; and (b) Sample 1-3 (Exposed).

compliance of the coatings. The top view of the molten deposits on the YSZ top coating of test sample 1-5 are shown in **Figure 5(b)**. The molten and cooled ash layer on top of the columns of the YSZ coating is thin, hardened, and almost glass-like.

A molten deposit infiltrated top coat has been found to be more susceptible to delamination, and spallation of the YSZ coating was found for the samples in the current study. A diagonal crack developed after sectioningalong the top surface of top coat of sample 1-7 (see **Figure 6(a)** The crack further propagated during sample preparation procedures and led to delamination of the TBC. **Figure 6(b)** & **Figure 6(c)** show that Sample 1-3 lost roughly 100 µm of YSZ coating near the edge where deposition was abundant.

In areas where deposition adhered onto the top surface of the YSZ coatings but did not cause delamination,

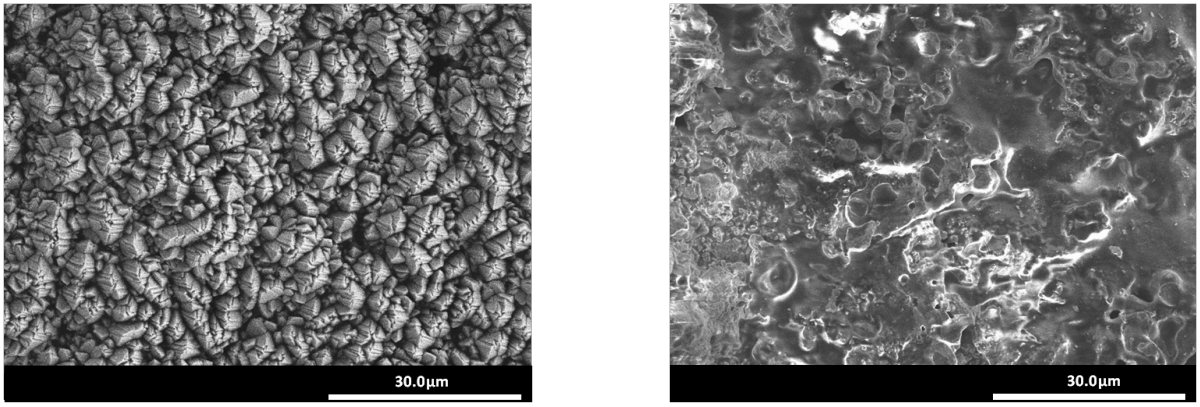

(a) (b)

Figure 5. Top view of (a) Unexposed Samples 2-1; and (b) Molten deposition on Sample 1-5 (Deposition Exposed) [15].

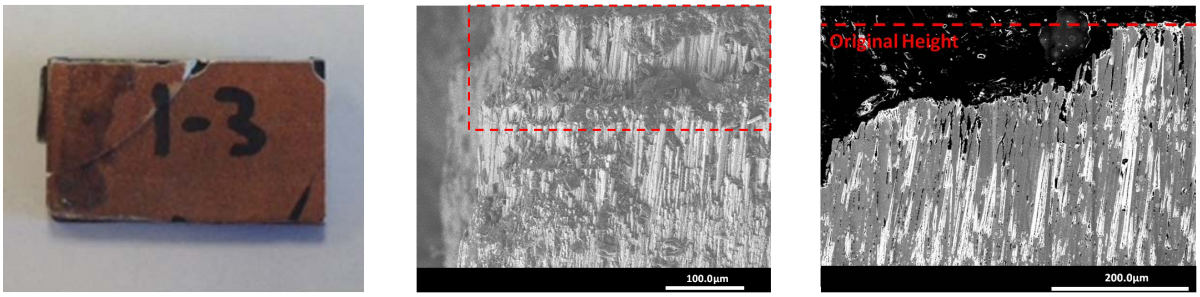

(a) (b) (c)

Figure 6. (a) Top view of sample 1-7 and cross-section micrographs of delamination in Sample 1-3 top coating; (b) After sectioning, post-sectioning; and (c) After mounting and polishing, mounted in a conductive mounting media [15].

the fly ash deposition did not infiltrate deep into the top coat. **Figure 7** shows the infiltration of the fly ash deposits into the TBC on sample 1-3. **Figure 7(a)** shows a cross-sectional micrograph of the top surface of sample 1-3. The dashed red line shows the original top surface of the 7YSZ coating. **Figure 7(b)** & **Figure 7(d)** shows corresponding Zr, Si, and Al EDS elemental maps, respectively. Silicon and aluminum are chosen for the elemental mapping since they contain the two highest elemental percentages that make up the composition of the fly ash. **Figure 7(a)** & **Figure 7(d)** shows that even the most heavily deposited test article only sees an infiltration depth into the YSZ coating of 10 - 20 µm.

A cross-section of sample 1-3 where a heavy amount of deposition is on top of the YSZ coating is shown in **Figure 8**. The image in **Figure 8(a)** is divided into four regions: epoxy, molten deposits, interaction zone, and unaffected YSZ. The elemental distributions of the latter three microstructural regions are listed in Table 2. The results are the average of several EDS Point & ID spectrum results at each columnar center and infiltration depth locations. The interaction zone is broken up into sub-regions Zone 1 and Zone 2 in **Figure 8(b)**. Zone 3 represents a YSZ depth relatively unaffected by the molten deposits. Silicon, aluminum, and iron comprise the three largest elements by percentage in the original processed fly ash. The molten deposits that lie on top have a comparable elemental distribution. The small change in the weight percentage between the processed fly ash and molten deposits was found in this study and was also found for the coal ash particulate in a study by Bons, Crosby, Wammack, Bentley, and Fletcher [17]. The detection of yttria and zirconia in the deposit layer indicates that some of the TBC has migrated into the molten fly ash deposit. Zone 1 is placed at the tips of the YSZ coatings, and although the spectrum results show that zirconia is the predominant element, there is still presence of the molten deposits on the column tips. The weight percentage level of yttria at roughly 5% is lower than the 7% - 8% normally found in 7YSZ. This agrees with the yttria migration into deposit layer found in the study by Peng *et al.* [16]. The study by Peng *et al.* completed the same type of EDS analysis using CMAS and an EB-PVD YSZ coating and showed yttria migration to the CMAS deposit. Zone 2 lies 10 µm into the columnar tips and shows just a trace amount of deposit elements in the YSZ of the zone. Zone 3 is 20 µm into the columnar

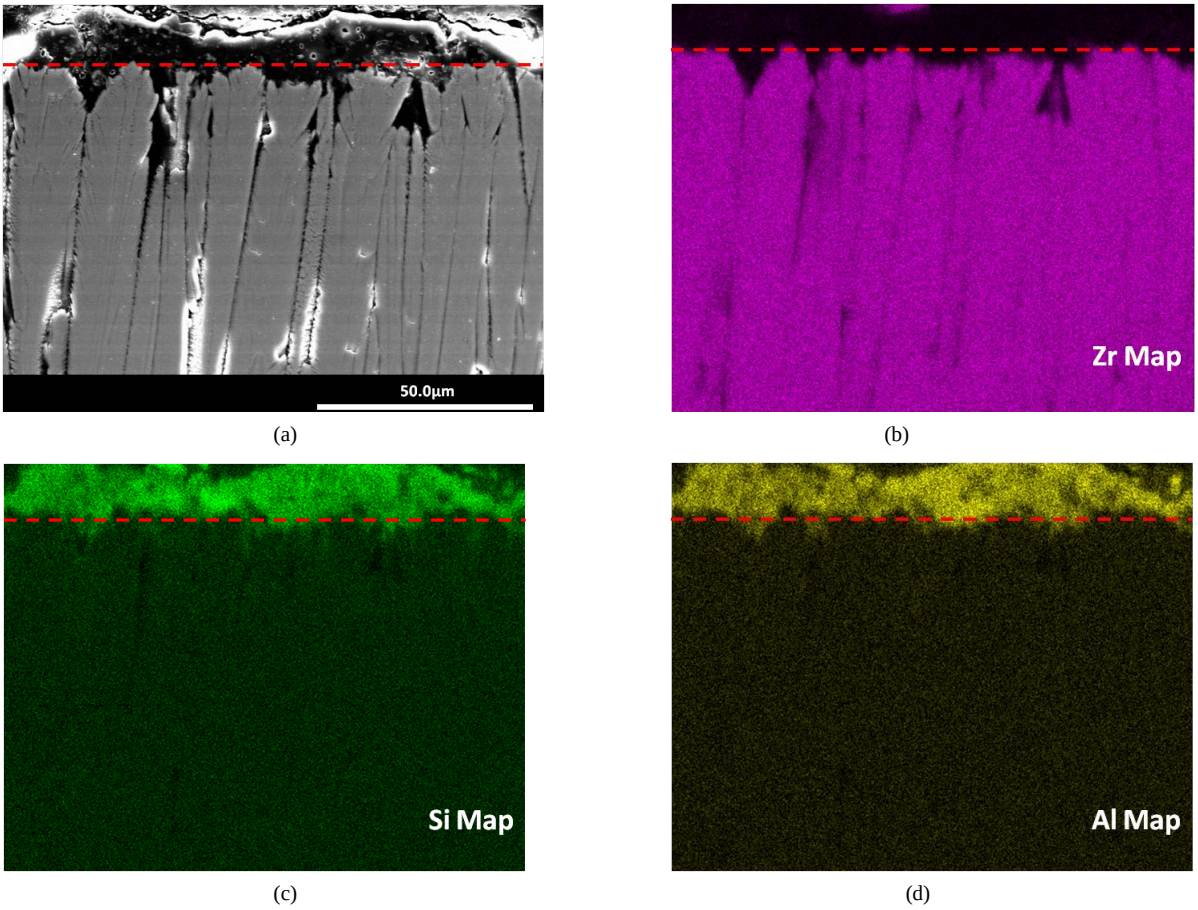

(a) (b)

(c) (d)

Figure 7. (a) Cross-section SEM micrograph of Sample 1-3 that has interacted with molten fly ash and corresponding elemental maps: (b) Zr, (c) Si, and (d) Al. The horizontal dashed lines denote the original top surface of the TBC.

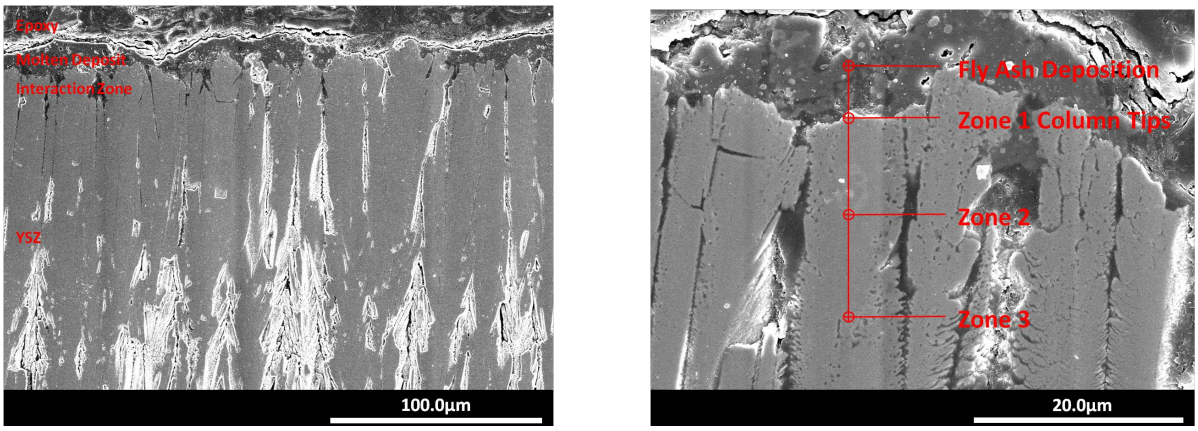

(a) (b)

Figure 8. Cross-section views of (a) TBC on sample 1-3 with molten deposits, their region description; and (b) Locations of EDS spectrum analysis.

tips and contains even less of the fly ash composition. The results in **Table 2** agree with the EDS maps in **Figure 7** for infiltration depth.

Figure 9(a) contains an illustration from Levi *et al.* [3] that allows visualization of the dissolution-reprecipitation mechanism of yttria-stabilized zirconia in CMAS. The ceramic coating material dissolves within the molten

Table 2. Elemental distribution (excluding oxygen) of the fly ash deposition and zones 1 - 3 in **Figure 8(b)**.

Constituent/wt.%	Si	Al	Fe	Y	Zr
Original Fly Ash	28.09	14.98	6.93	-	-
Molten Deposit	23.23	12.98	5.76	1.35	9.54
1 (Column Tips)	5.77	4.44	1.83	5.24	56.87
2 (10 μm)	0.66	0.03	0.35	6.74	75.32
3 (20 μm)	0.53	0.01	0.21	7.31	77.04

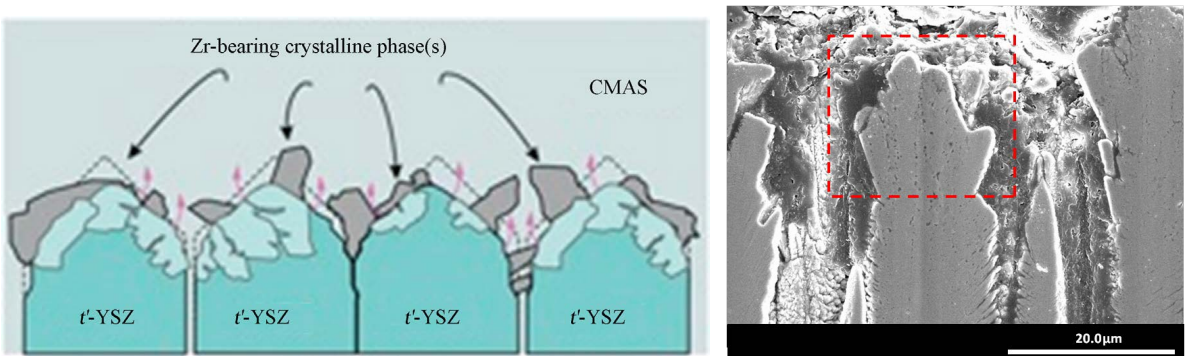

(a) (b)

Figure 9. (a) Schematic illustration of the dissolution-reprecipitation mechanism in YSZ [4] and (b) SEM micrograph of a reprecipitated YSZ columnar tip of sample 1-3.

glass and reprecipitates in one of the modified crystalline phases of the YSZ as the yttria is leeched out of the YSZ. **Figure 9(b)** contains a micrograph of a YSZ columnar tip in sample 1-3 that was reprecipitated in the molten fly ash deposit. The column tips have lost their identity. The molten fly ash does have similar degradation to the ceramic top coat tips as the molten glass from CMAS. The reprecipitated YSZ columnar tips, along with the stress mismatch caused by the molten deposit, may have attributed to the strain tolerance loss found in the study of the mechanical properties of the test samples [15]. Further penetration of the deposition and heat treatment can result in floating YSZ in the deposits leading to the appearance of globular particles found in studies by Levi *et al.* [3] and Peng *et al.* [16].

4. Conclusions

This purpose of the current study was to analyze the microstructure of TBC coating systems on the test articles used in the Murphy, Nix, Lawson, Straub, and Beer study after 6-hour (accelerated to simulate of 10,000 hours) syngas particulate deposition. The articles were sectioned, mounted, and polished to study the microstructure of selected areas of varying quantities of deposition. Scanning electron microscopy and energy dispersive X-ray spectroscopy was used to characterize the TBC coatings at a microscopic level.

The molten deposits from the fly ash was found to penetrate the inter-columnar gaps of the YSZ a shallow depth of 10 - 20 μm, but the deposits still lead to degradation of the DVD YSZ layer of TBC. Once the deposits were cooled on the top coat, the YSZ layer had a higher tendency to delaminate. SEM and EDS work showed that the deposit/YSZ interaction zone dissolved and reprecipitated the column tips of the top coating and made the tips lose their identity. During the dissolution-reprecipitation of the YSZ coating, the stabilizing yttria from the top coat column tips within the interaction zone is absorbed by the fly ash deposition, causing phase transformations within the YSZ. The phase transformation changes the mechanical and thermal properties in the YSZ coating.

Acknowledgements

The authors would like to acknowledge the support of the Department of Energy, Office of Science, Experimental

Program to Stimulate Competitive Research (EPSCoR) under grant/contract number DE-FG02-09ER46615, monitored by Dr. Tim Fitzsimmons. In addition, with a cooperative agreement with EPSCoR, the project was partially funded by the US Department of Energy, National Energy Technology Laboratory. There are several people that deserve acknowledgments for their contributions to this project. The authors would like to thank Dr. Keith Kruger of Haynes, International for donating the Haynes 230 test article material. The thermal barrier coatings that were applied were cost shared by Dr. Derek Hass and Balvinder Gogia of Directed Vapor Technologies International, Inc. (DVTI). In addition, DVTI applied the bond coat to the test articles. Westmoreland Mechanical Testing & Research, Inc. sectioned the angled test articles into the test samples. Mounting and polishing of the samples were completed by Metallurgical Technologies, Inc. Gratitude also goes out to the Shared Research Facilities and the Chemical Engineering Department at West Virginia University for the cleanroom access, training, and use of the SEM and other metallurgical preparation machines.

References

[1] Padture, N.P., Gell, M. and Jordan, E.H. (2002) Thermal Barrier Coatings for Gas-Turbine Engine Applications. *Science AAAS*, **296**, 280-284. http://dx.doi.org/10.1126/science.1068609

[2] Schulz, U., Leyens, C., Fritscher, K., Peters, M., Saruhan-Brings, B., Lavigne, O., Dorvaux, J.-M., Poulain, M., Mévrel, R. and Caliez, M. (2003) Some Recent Trends in Research and Technology of Advanced Thermal Barrier Coatings. *Aerospace and Technology*, **7**, 73-80.

[3] Levi, C.G., Hutchinson, J.W., Vidal-Sétif, M.-H. and Johnson, C.A. (2012) Environmental Degradation of Thermal-Barrier Coatings by Molten Deposits. *MRS Bulletin*, **37**, 932-941. http://dx.doi.org/10.1557/mrs.2012.230

[4] Wellman, R.G. and Nicholls, J.R. (2000) Some Observation on Erosion Mechanisms of EB PVD TBCs. *Wear*, **242**, 89-96. http://dx.doi.org/10.1016/S0043-1648(00)00391-4

[5] Drexler, J.M., Gledhill, A.D., Shinoda, K., Vasiliev, A.L., Reddy, K.M., Sampath, S. and Padture, N.P. (2011) Jet Engine Coatings for Resisting Volcanic Ash. *Advanced Materials*, **23**, 2419-2424. http://dx.doi.org/10.1002/adma.201004783

[6] Murphy, R.G., Nix, A.C., Lawson, S.A., Straub, D. and Beer, S.K. (2012) Preliminary Experimental Investigation of the Effects of Particulate Deposition on IGCC Turbine Film-Cooling in a High-Pressure Combustion Facility. *ASME Turbo Expo* 2012: *Turbine Technical Conference and Exposition*, **4**, 979-986. http://dx.doi.org/10.1115/GT2012-68806

[7] Hass, D. (2012) Thermal Barrier Coating Environmental Durability Enhancement (CMAS). *NAVAIR*, **N06-032**.

[8] Gleeson, B., Wang, W., Hayashi, S. and Sordelet, D.J. (2004) Effects of Platinum on the Interdiffusion and Oxidation Behavior of Ni-Al-Based Alloys. *Material Science Forum*, **461**, 213-222. http://dx.doi.org/10.4028/www.scientific.net/MSF.461-464.213

[9] Dorrington, J.R., Bogard, D.G. and Bunker, R.S. (2007) Film Effectiveness Performance for Coolant Holes Imbedded in Various Shallow Trench and Crater Depressions. *ASME Turbo Expo* 2007: *Power for Land, Sea, and Air*, **4**, 749-758. http://dx.doi.org/10.1115/GT2007-27992

[10] Bons, J., Ameri, A. and Fletcher, T. (2012) Designing Turbine Endwalls for Deposition Resistance with 1400C Combustor Exit Temperatures and Syngas Water Vapor Levels. The Ohio State University. http://dx.doi.org/10.2172/1080354

[11] Lawson, S.A. and Thole, K.A. (2011) Effects of Simulated Particle Deposition on Film Cooling. *Journal of Turbomachinery*, **133**, Article ID: 021009. http://dx.doi.org/10.1115/1.4000571

[12] Dennis, R.A., Shelton, W.W. and Le, P. (2007) Development of Baseline Performance Values for Turbines in Existing IGCC Applications. *ASME Turbo Expo* 2007: *Power for Land, Sea, and Air*, **2**, 1017-1049. http://dx.doi.org/10.1115/GT2007-28096

[13] Murphy, R.G. (2012) Experimental Investigation of Particulate Deposition on a Simulated Film-Cooled Turbine Vane Pressure Surface in a High Pressure Combustion Facility. M.S. Thesis, West Virginia University, Morgantown.

[14] Murphy, R.G., Nix, A.C., Lawson, S.A., Straub, D. and Beer, S.K. (2013) Investigation of Factors That Contribute to Deposition Formation on Turbine Components in a High-Pressure Combustion Facility. *ASME Turbo Expo* 2013: *Turbine Technical Conference and Exposition*, **3B**, V03BT13A027.

[15] Luo, K., Nix, A.C., Kang, B.S. and Otunyo, D.A. (2014) Effects of Syngas Particulate Fly Ash Deposition on the Mechanical Properties of Thermal Barrier Coatings on Simulated Film-Cooled Turbine Vane Components. *International Journal of Clean Coal and Energy*.

[16] Peng, H., Wang, L., Guo, L., Miao, W., Guo, H. and Gong, S. (2012) Degradation of EB-PVD Thermal Barrier Coatings Caused by CMAS Deposits. *Progress in Natural Science*: *Materials International*, **22**, 461-467.

http://dx.doi.org/10.1016/j.pnsc.2012.06.007

[17] Bons, J.P., Crosby, J., Wammack, J.E., Bentley, B.I. and Fletcher, T.H. (2007) High-Pressure Turbine Deposition in Land-Based Gas Turbines from Various Synfuels. *Journal of Engineering for Gas Turbines and Power*, **129**, 135-143. http://dx.doi.org/10.1115/1.2181181

Scientific Research Publishing (SCIRP) is one of the largest Open Access journal publishers. It is currently publishing more than 200 open access, online, peer-reviewed journals covering a wide range of academic disciplines. SCIRP serves the worldwide academic communities and contributes to the progress and application of science with its publication.

Other selected journals from SCIRP are listed as below. Submit your manuscript to us via either submit@scirp.org or Online Submission Portal.